Arab J Geosci
DOI 10.1007/s12517-015-1914-4

ORIGINAL PAPER

Determination of Kula basalts (geosite) in Turkey using remote sensing techniques

Ozsen Corumluoglu[1] · **Alaaddin Vural**[2] · **Ibrahim Asri**[1]

Received: 25 July 2014 / Accepted: 7 April 2015

Abstract Kula Region (Manisa, Turkey), with its 80 volcanic cones, lava flows, basalt plateaus and basalt columns, fairy chimney formations in canyons carved by the Gediz River, shelter cities hidden in volcanic lava, footprint fossils belonging to the first humans, and geological uniqueness, has a great importance in terms of geotourism potential as it is being a natural heritage in the Aegean region of Anatolia. In this study, some remote sensing image processing techniques such as band combination, band rationing, and principal component analyses were used to depict the cultural and natural geosite known as Kula basalts in Turkey. Satellite images utilized here in this study were Landsat band images (band 1 to band 7). Principal component analyses (PCA) were performed on the first ratio group with 5/4, 5/1, and 3/7 bands and then on the second ratio group with 3/1, 4/5, and 3/2 bands. As a conclusion and outcome of this PCA, it was found that red, green, and blue (RGB) composite with PC1 and PC3 gray-level images from the first ratio group and PC2 gray-level image from the second group showed up the basalt areas better than those from other techniques studied in this research. After unsupervised classification of this final composite of PCA, it is computed that the basalt rocks in Kula cover an area of 36,774 ha totally.

✉ Alaaddin Vural
vural@gumushane.edu.tr

Ozsen Corumluoglu
ocorumlu@hotmail.com

Ibrahim Asri
ibrahim.asri@ikc.edu.tr

[1] Department of Geomatics, Izmir Katip Celebi University, Izmir, Turkey

[2] The Department of Geological Engineering, Gümüşhane University, Faculty of Engineering and Natural Sciences, Gümüşhane, Turkey

Keywords Remote sensing · Principle component analysis (PCA) · Band ratio · Kula basalt · Geosite

Introduction

In general meaning, each rock type with its characteristic rock-forming minerals has its own reflectance signature, and thus by using the remote sensing techniques, the different rock types in a particular area can be reasonably discriminated on the basis of their reflectance characteristics (Hassan and Ramadan 2014). The importance of the recognition of such spatial patterns of rocks makes the remote sensing techniques as one of the standard procedure in geological studies, due to its speed and price.

This study aims to examine the subterranean pathways used by the erupted products of the cinder cones of the Kula Volcanic Field, Manisa, in Western Turkey (Richardson-Bunbury 1996). The basaltic lavas which used these pathways contain cognate nodules, thought to represent partially solidified fractions of the magma (Holness 2005; Holness and Bunbury 2006) which were brought to the surface later in the same eruptive period.

The Kula region (in the northwest of Turkey), as a volcanic field and as a natural asset of Anatolia, is also hosting numerous historical and archaeological sites. Therefore, the main purpose of this study may be emphasized as that Kula basalts as a natural world heritage in Turkey would be determined, delineated, and computed with their total coverage in the region using the most appropriate remote sensing image analysis technique found as composite image of PCs from several PCAs of certain Landsat band ratios. To reach this purpose, a final map representing Kula volcanic field was produced after several remote sensing image analyses. Thus, the lithological characteristic of the area was identified as an outcome of remote

Published online: 19 April 2015

sensing data processing methods, and ratio images such as 3/1, 4/5, and 3/2 from Landsat Enhanced Thematic Mapper (ETM+) bands showed up the basaltic areas better than other ratio combinations in the region. Images from principal components analysis (PCA), along with ratio images, were computed and then combined to determine the response of minerals. PCA image combination of 3/1, 4/5, and 3/2 ratios, in red, green, and blue, appeared as a best outcome displaying and mapping the boundaries of the main lava flows in the geosite. Remote sensing is an important data source for mapping the past volcanic activities, but can also be used as the sources of archaeological structures and architectures in volcanic areas such as those in the Kula volcanic field.

The Kula region

The Kula Volcano (Turkey, 38.58° N and 28.52° E) was active in the Quaternary period and now it is inactive. The site is located 12 km west of the Kula town and 1.5 km in the north of Izmir-Ankara highway at the altitude of 750 m. It covers an area of approximately 400 km^2 with no vegetation in general except some areas. It includes three basins, and the schistose ridges separating them are covered with volcanic cones and lava streams and fields.

As indicated in Ercan's paper (1984), "the Quaternary Kula volcanic are Na-dominant in character while all the older volcanic rocks of western Anatolia are generally definitive K-dominant rocks. As a unique example in western Anatolia, the existence of a huge amount of plateau basalts at Kula indicates rapid uplift of mantle material, as confirmed by new geochemical data." The basement rocks in the area laying between Kula and Salihli towns in the province of Manisa consist mainly of gneisses, schists and quartzites with Permo Triassic marbles in the uppermost section. Mesozoic units consists of dolomitic limestones of Jurassic and ophiolitic melange of Upper Cretaceous age. Senozoic units consist of fluvial sediments of Pliocene age overlain by andezitic lava flows with interfingering lacustrine limestones toward the top. Kula volcanics of Quaternary age flowed in three main periods; the initial products were being ejected 1.1 million years ago. The last period of volcanism lasted until historic times. According to petrographic and petrochemical investigations, Kula lavas are alkali basalts. Most of the rock types are trachy basalts, alkali olivine basalts, and hawaities with minor mugearites and tephrites. Kula volcanism has a mantle origin derived from an initial magma rise through plums, and it is a rift volcanism (Ercan 1984).

Based on their field observations, Tokcaer et al. (2005) indicates those in their paper; the oldest Kula volcanics are the plateau basalts with more than one main lava flow. At the beginning of volcanic activity (first-period plateau basalts), this plateau was vast. Subsequently, parts of the first-period plateau basalts were uplifted and partly eroded while other parts were covered by younger lavas, tephra, and sediments. The horsts, covered by plateau basalts, are well protected because of their resistance to erosion. During extensional activity, the development of cinder cones continued without hiatus. During the last period of volcanic activity, the youngest craters once again produced lava flows to form the second-period plateau basalts. As a result, there are more than 80 cinder cones with quite different erosional stages between the first and second plateau basalt periods. The Kula basalts are the only example of rapid uplifting of asthenospheric material in western Anatolia and are interpreted to form due to the opening of a horizontal slab window as a consequence of the more rapid southwestward movement of the Aegean microplate overriding Africa, with respect to the Anatolian plate (Tokcaer et al. 2005).

Remote sensing in geological mapping and mineral exploration studies

In early times, geological maps were produced after a fieldwork like traversing, but today, remote sensing technology as a complicated method which is cost-effective has been approved in terms of its capacity to work with classic geologic mapping. Remote sensing has been realized as a technologically advanced data-obtaining method for geology; the technique is normally used in determination of Earth's surface geological structure and features such as lithology, lithological sequences, relative age of rock strata, types of drainage, soil type, and vegetation cover (Drury 1993; El Janati et al. 2014). If this technique is used together with maps for ground truth, this turns classical geological mapping into more effective and efficient mapping process.

Remote sensing techniques have been applied for years and new methodological perspectives are still being developed by using this high technology. Remote sensing methods require mapping the zone accurately. Different alteration types can be identified by multispectral data, and the lithological boundaries of the basaltic rocks can also be delineated exactly by remote sensing data analyses as suggested here in this study.

Remote sensing techniques are of valuable use in mapping hydrothermally altered minerals that have distinct absorption features (Hunt 1979). Multispectral remote sensing sensors provide detailed information on the mineralogy of different rock types of the Earth's surface and have been used by several scientists (Crosta and Moore 1989; Abdelsalam et al. 2000; Rokos et al. 2000; Ferrier et al. 2002; Crosta et al. 2003; Youssef et al. 2009; Qari 2011; Salem et al. 2014). Several authors utilized the remote sensing techniques for (1) mapping hydrothermally altered minerals (e.g., Abdelsalam et al. 2000; Kusky and Ramadan 2002; Liu et al. 2007; Madani et al. 2003; Ramadan and Kontny 2004; Ramadan et al. 2001; Sultan and Arvidson 1986) and (2) mapping the local fractures and lineaments that controlled

the mineralization (e.g., Madani and Bishta 2002). Abdelsalam et al. (2000) employed the 5/7, 4/5, and 3/1 band ratio image in red, green, and blue (RGB) for mapping the alteration zone of Beddaho in northern Eritrea. Ramadan et al. (2001) mapped the alteration zone associated gold-bearing massive sulfide deposits of Allaqi suture, South Eastern Desert of Egypt, using Landsat TM color composite ratio images. Ramadan and Kontny (2004) utilized the Landsat TM band ratios and detected two types of alteration zones that are controlled by NW–SE structural trend at Shalatein District, South Eastern Desert of Egypt. Madani et al. (2008) studied the Landsat ETM+ data using band ratio technique for mapping the listwaenite exposures along the southern margin of Jabal Al-Wask serpentinites, western Saudi Arabia.

In geological remote sensing studies, near-infrared (NIR), mid-infrared (MIR), and shortwave infrared (SWIR) portions of electromagnetic spectrum are generally used. One of the remote sensing data that is available and provides such spectral bands is Landsat data. Therefore, Moore et al. (2007) in his Clark Area Soil Survey study utilized Landsat 7 data to determine the quantity of basaltic rock outcrops. Moreover, remote sensing is becoming a widely applied mineral exploration technique day by day. There are several studies on geological exploration and determination of hydrothermal alteration zones in the literature using Landsat Enhanced Thematic Mapper (ETM^{+}) and Advanced Space borne Thermal Emission and Reflection Radiometer (ASTER) images (Buckingham and Sommer 1983; Kaufmann 1988; Drury and Hunt 1989; Carranza and Hale 1999; Crosta et al. 2003; Assiri et al. 2008; Warner and Farmer 2008). In remote sensing's geological applications and studies especially in geological and structural data interpretation, some difficulties are encountered such as signal deterioration because of different surface conditions such as vegetation, agricultural activities, and weathering crust (Drury 1993). Therefore, error and noise removing procedure became a routine process before any interpretation of remote sensing data. In remote sensing data analyses of geological studies, band rationing is used as a common method to reduce haze and vegetation cover effects (Carranza 2002). For example, Landsat ETM band 5 and band 7 and their ratio have been used successful for the discrimination of different rock types (lithological differences) and determination of hydrothermal alteration zones, and a ratio is also an image with minimized or removed errors (Crosta and Moore 1989; Drury 1993; Carranza and Hale 1999; Ferrier et al. 2002; Crosta et al. 2003; Moore et al. 2007; Bishta et al. 2014).

Material and methods

Several image processing techniques can be carried out, including image enhancement, band combination, rationing, and feature-oriented PCA as being used in Crosta technique (Abrams et al. 1983; Chavez 1989; Rowan and Bowers 1995; Sabins 1999; Gupta 2003; Ranjbar et al. 2004; Rawashdeh et al. 2006; Rajesh 2008; Pournamdari and Hashim 2014). During the image processing, a simple to complex stepwise path is followed. The resulting images are considered to be the potential geological/alteration maps. If the results display any convergence with the data from study area, then the final (combination) map is formed for displaying the convergence.

Satellite data

Landsat 7 ETM+ scene throughout the remote sensing image analysis to map the Kula volcanic complexes was the scene with orbit and section numbers of 180/33. Six ETM^{+} spectral bands of Landsat 7 acquired on 20th of August 2006 were used in remote sensing analyses. The remote sensor data that is commercially available is already systematic error removed; however, non-systematic error remains in the image (Jensen 1996). The image data is accepted as free from geometric errors, and ETM+ bands of 1, 2, 3, 4, 5, and 7 are used extensively in most of the processes. The approach of "identification of mineral assemblage for lithological mapping" (Gupta 2003) was adapted to distinguish the different units within the Quaternary volcanic formations. This approach depends on the broad spectral characteristics of minerals. The use of solar reflection of the region allows mapping of the iron and hydroxyl bearing surface of the basaltic rocks and, thus, to map the lithological boundaries of the main lava flows. Several remote sensing image processing methods were examined to obtain the final product images and to set up the map of the studied zone.

Band compositing

The idea behind the band combination is to make multispectral information visible to the human eye. Every object in nature has unique reflectance values at different wavelengths. On the other hand, the colors that the human eye can see are only the combination of the reflectance at red, green, and blue portions in the visible wavelength region. So that, multispectral images are assigned to the wavelengths (red, green, and blue, RGB) that are sensible for human. Color composite method is simply the decision of the order of three multiple bands to be displayed in red, green, and blue channels. That is why RGB composition of Landsat 7 ETM^{+} band 3, band 2, and band 1 is called true color composition (TCC), as it displays the image most likely as it is seen in nature to the human eye. All the other band compositions displayed as RGB are called false color composition (FCC) (Vincent 1997).

The color composition, in fact, is the basis of the other techniques, because the results can be easily interpreted in detail with color composites by assigning the desired spectral

band to the desired RGB channel. Therefore, there are a large number of studies concerned on the best combination of bands to display the maximum information about the surface lithology and mineralogy.

With respect to the literature, it is also found that some statistical methods used in remote sensing image processes are defective in a way that they ignore the distinction between geologically significant variance (color differences between or within rock types) and non-geological factors (differences in topography and shadow for surfaces with high and albedo, and differences between rock, vegetation, alluvium, etc.). It is found to better assess each band individually by eye and choose the best three having the likely diagnostic features (Rothery 1987).

Most of the previous studies done for the determination of alteration rocks showed that the hydroxyl absorption band in Landsat bands is band 7 and a general reflectance high band is band 5. The bands 7, 4, and 5 combined in RGB were decided as the most informative image for lithologic features of surfaces and alteration areas. So, pillow basalt lavas are observed in dark grayish magenta whereas gabbros have a green tone (Rothery 1987) (Fig. 1a).

In addition to that, RGB color composites of TM bands 741, 541, and 531 can also be selected according to the index of optimum band selection criteria. On the other hand, TM472 and TM475 color composite images are emphasized as the most informative images for discriminating the clay minerals in the literature, and the same procedure was followed in this study as well (Fig. 1b, c). Radiometric enhancement is even found to be very helpful for visual analysis of RGB color composites which is performed by different methods like linear contrast stretching, histogram equalization, and decorrelation stretching (Chica-Olmo and Abarca 2002).

RGB display of bands 4, 7, and 2 makes the structural elements identifiable and allows discrimination of surficial units like sedimentary and volcanic rocks. Light reddish and grayish brown color represents granites and grayish green colors represent monzogranite as Abdelhamid and Rabba (1994) stated in his work.

Based on the statistical results of average factoring, standard deviations and interband correlations of TM bands 2, 3, 4, 5, and 7, and combination of bands 4, 7, and 2, and 3, 7, and 4 are selected for color composite in RGB order of channels. Color composite of bands 4(R), 7(G), and 2(B) displayed iron oxides as yellowish green; 3(R), 7(G), and 4(B) composite displayed again iron oxides as light green. Since they show almost similar pattern of RGB image, here 3, 7, and 4 band combination images are also given in Fig. 1b, d.

Band ratioing

Band ratioing depends on division of one spectral band by another one in a multispectral scene. This division results in the ratio of spectral reflectance measured in the one spectral band to the spectral reflectance measured in another spectral band. Thus, band ratio technique highlights the spectral differences related to the specific materials to be mapped and disintegrates these surface materials from each other; otherwise, such information will not be available in any single band (Jensen 1996). The outcome image is in gray levels, and to improve its display quality in the whole range of 256 gray levels, it is stretched. The best stretching method used for

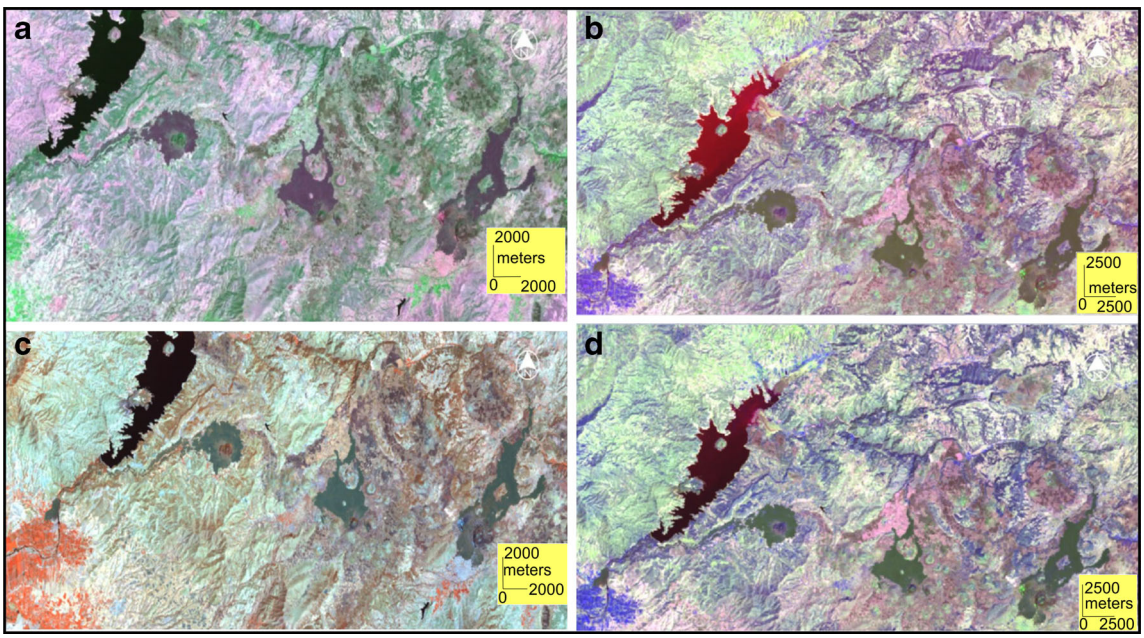

Fig. 1 **a** RGB color composite image of Landsat bands 7, 4, and 5. **b** RGB color composite image of Landsat 4, 7, and 2 bands. **c** RGB color composite image of Landsat 4, 7, and 5 bands. **d** RGB color composite image of Landsat 3, 7, and 4 bands

these ratio images here in this study was the normalized contrast stretching.

As it is mentioned previously, band ratios are obtained easily by dividing digital number of each pixel at the one location in one band by the each pixel at the same location in another band. Moreover, as reported by Drury (1993) and Darning (1998), ratios like 3/1, 3/5, 3/7, 5/1, 5/4, 3/7, and 5/7 have great success on the determination of lithologies, and with this fact in this study, some of these ratios were used to differentiate and identify rock types. It is also found that the combined RGB image consisted of ratio images of 5/4, 5/1, and 3/7 represented the best result for the basalt rocks in reddish colors (Fig. 2a).

The RGB display in Fig. 2a shows identical results with Abrams et al.'s (1983). The contrast in the resulting image displayed dark-toned unaltered rocks, in shades of dark blue and green, and hydrothermally altered rocks, displayed in bright yellow to orange, coinciding with the preliminary mapped phyllic-potassic zones. However, discrimination between phyllic and potassic alteration zones could not be made. So, granite outcrops are mapped as reddish areas as well as obtained in Abrams et al.'s work (1983).

When band ratios of 1.65/2.2 μm, 0.66/0.56 μm, and 0.83/1.65 μm which correspond with band ratios of 5/7, 3/2, and 4/5 are assigned to the red, green, and blue channels, iron-oxide-rich areas are displayed as green due to the presence of ferric iron charge transfer band in the ultraviolet, and clay-rich areas are displayed as red, due to the presence of the hydrous minerals absorption band near 2.2 μm. Yellow or orange areas represent the areas where both clay and iron oxide minerals are present (Abrams et al. 1983). When the same image processing was applied to the Landsat bands used in this study, the combined RGB image consisting of 5/7, 3/2, and 4/5 ratio images showed the similar results after histogram stretching with ignored zero values in statistic process. Basalts are displayed in greenish color as seen in Fig. 2b.

Band 4 normally highlights vegetation which is having high reflection values in this band; contrary to this, the other bands are better in reflections and absorptions from rock forming minerals like oxides and hydroxyls (Carranza 2002). Especially, band ratio 4/3 therefore represents vegetation in bright tones because of the high reflectance of mesostructure in the NIR band against the steep falloff of reflectance in the visible TM3 band due to intense chlorophyll absorption (Kaufmann 1988). A set of ratios are therefore selected reflecting the spectral behavior of iron oxides, minerals containing OH, H_2O, CO_3, and SO_4 molecules, and vegetation. Additionally, due to the high rock discrimination feature of the color composite, images like 3/1, 5/7, and 3/5, and 4/5, 6/7, and 4/6 used and represented in red, green, and blue by Rowan et al. (1977) and Raines et al. (1978) have also been examined in this study.

Clay minerals containing water (bound or unbound), micas, carbonates, sulfates, and hydrates are enhanced by the band ratio 5/7. The ferric and ferrous iron is best enhanced by the band ratios 7/4, 7/1 or 5/4, and 5/1, due to major electronic transition bands in NIR (at ~0.87 μm) and the visible and charge transfer bands in ultraviolet and the unaffected SWIR range (Kaufmann 1988). Mostly used band ratio 3/1 often fails because the difference between bands 3 and 1 is

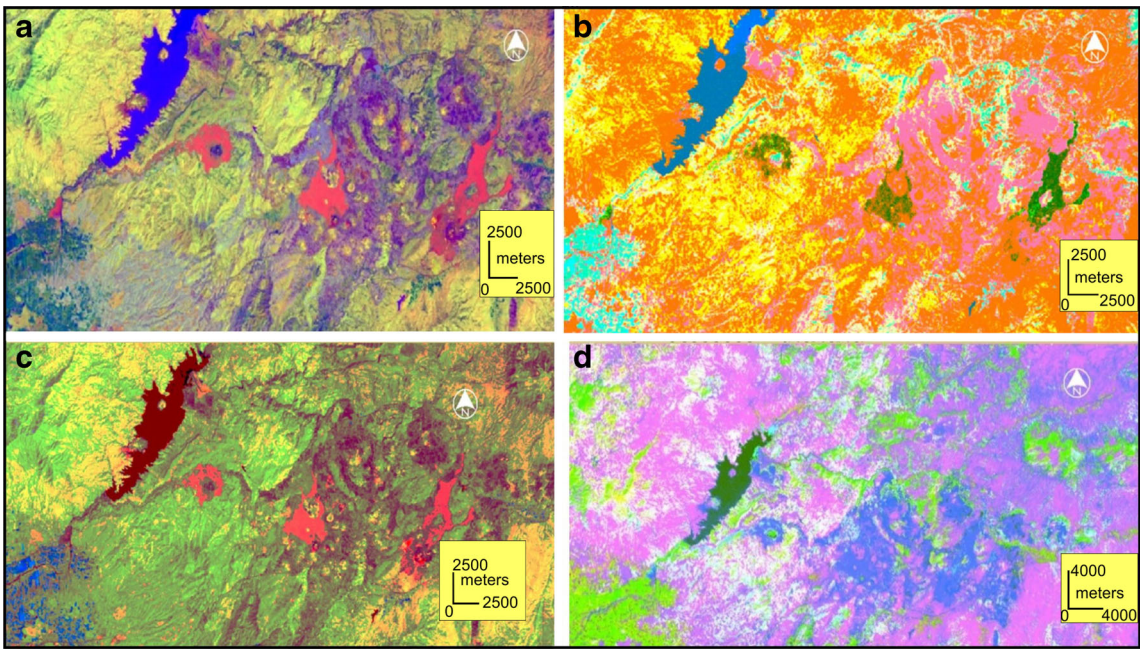

Fig. 2 **a** RGB color composite image of 5/4, 5/1, and 3/7 ratios. **b** RGB color composite image of 5/7, 3/2, and 4/5 ratios after histogram stretching. **c** RGB color composite image of 7/4, 5/1, and 4/3 band ratio. **d** RGB color composite image of 5/1, 5/7, and 7/4 band ratio

much less than those in the combinations of SWIR bands like bands 1 or 4. Among all of those ratio images above, the best RGB ratio image displaying Kula basalts is obtained as the one using band ratios of 7/4, 5/1, and 4/3, and they appear as pastel red color in the product image (Fig. 2c).

Landsat TM 5/7 band ratio is the best spectral ratio emphasizing iron-rich rocks and rocks with clays and hydroxyl minerals which show high reflectance in band 5 and low in band 7. Therefore, clay-rich rocks as it has been reported by Darning (1998) are clearly identified in the ratio image 5/7 using these bands, and they appear as light pixels in gray scale colors.

A RGB color composite image was also created using band ratios of 5/1, 5/7, and 7/4 after a histogram stretch with ignored zero values (Fig. 2d). Consequently, pink color represents the minerals containing iron ions, green represents the vegetated zones, and blue represents OH/H_2O-, SO_4-, or CO_3-bearing minerals (rocks and soils) (Kaufmann 1988). But, basalts might not easily be identified in the ratio scene even after histogram stretching (Fig. 2d).

The proportions of kaolinite, illite, and free iron increase from the contact toward the granite intrusion, while the proportions of chlorite and smectite decrease. Reflectance spectra of soil samples from laboratory observations indicate that brightness decreased in the band ratios 3/2, 2/5, and 2/7 while it increased in 3/4, 4/7n and 5/7 ratios with the increase of the proportion of kaolinite, illite, and free iron and the decrease of chlorite (Kaufmann 1988).

TM band ratio of 5/7 is found very effective in highlighting clay minerals; 5/4 and 3/1 enhanced the areas with iron minerals and ferric oxides, respectively. RGB composite image of 5/7, 4/5, and 3/1 ratios reveals the main geological features in the studied region (Chica-Olmo and Abarca 2002).

The RGB color composite of 5/7, 3/1, and 5/4 ratio images maps the granite and the volcanics in dark blue to blue and violet-blue, reflecting the presence of Fe and Mn oxides. Also, the color composite of TM 3/1, 5/7, and 4/5 band ratios assigned to RGB channels after histogram equalization clearly displays the distribution of highly altered zones in dark blue to violet-blue colors (Abdelhamid and Rabba 1994).

After all the ratios given above were examined, it was found that the best RGB combination was 3/1, 4/5, and 3/2 ratio image combination for the basalts in the region, and the basalts clearly appeared in dark blue color as seen in Fig. 3a. In the unsupervised classification image, basalt areas are represented in red color. But, some noise spots and small areas in the close vicinity of the main basalt areas are appeared in red too as seen in Fig. 3b.

Principal component analysis

The principal component process is the principal component transformation technique to reduce dimensionality of correlated multispectral data. The technique is applied to a few to many correlated rasters to create a lesser number of images with more number of information than those in previous each image.

In a plot of the spectral band values that contain most of the variability in the data set, the data delineates an ellipse, and the original axes and origin do not fit the data distribution very well. Moving the origin of the mean values of the two data sets will surely give the axes a better fit to the data. Data is then translated, that is rotated, the major axis with respect to the new origin. The first principal component axis runs along the major axis of the ellipse standing for most of the variability in the data set. The minor axis as a second principal component axis is orthogonal to the major axis, and it is aligned along the maximum remaining variance. The variances of the principal components are called eigenvalues. Therefore, the maximum amount of remaining variance, which becomes smaller as the order of the principal component increases, is removed by each subsequent principal component, orthogonal to all the other principal components. Consequently, the nth component contains all of the remaining variance and separates the most spectrally unique pixels from the rest of pixels in the image. The total variance of all principal components sums up to 100 % of the total variance of the data, with the first three PCs usually accounting the majority (50–95 %) of the variance, when $n>3$.

Principal component analysis consists the translation of the origin and rotation of the data axes to better fit the brightness values of the input images. Each input object is a coordinate axis and each output object is a principal components axis.

In other words, principal component transformation consists of a two-step process. In the first step, n histograms of the scene to be imaged are used as inputs to the principal component algorithm. This algorithm calculates n principal components, which are actually orthogonal vectors in n-dimensional space that are oriented along directions of maximum remaining variance. Most of the variability in the information in the input objects is found in two or three of the objects. The other input objects contain decreasing amounts of the variance in the information set.

The second step consists of the transformation of the image to principal component space. The first principal component displays the greatest variance and highlights sunlit slopes rather than shadowed areas. The nth principal component image usually gives the homogeneous image, interrupted by a few bright and dark pixels that are spectrally unique for that image scene.

It is possible to create a color composite by using the desired 3 of the n PCs, when $n>3$. As most of the variance is represented by the first three principal components, they are used as a color composite to observe boundaries between terrain units. Color composites of the higher-order principal component images, including the nth one, make it possible

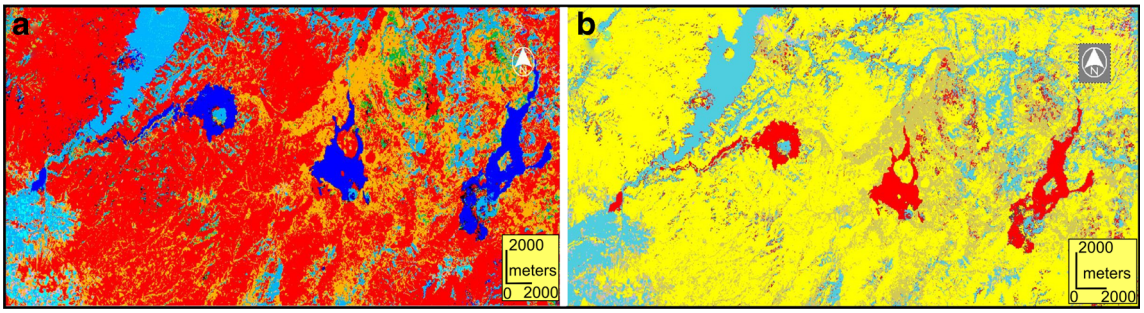

Fig. 3 **a** Combined RGB image of 3/1, 4/5, and 3/2 ratios after histogram stretching. **b** Unsupervised classification image of histogram stretched ratios of 3/1, 4/5, and 3/2

for the small areas on the ground that are spectrally outrageous to be identifiable (Vincent 1997).

For Landsat six bands' TM images, when information is transformed to three PCA images, all of the variance from the set of input objects are almost included in these three images. Since interpretation of these original PCA data is not easy, a combined RGB image can be formed from those three images to ease the interpretation. Also, transformation makes unseeing details in the raw data clearly be seen.

Feature-oriented PCA (Crosta technique)

Even if a great amount of information is gathered in reduced amount of images from PCA, certain materials will not be mapped; the likelihood that others will be mapped increases into only one of the principal component images. One of the successful PCA techniques used in remote sensing is suggested by Crosta and Moore (1989) and thus known as Crosta technique. In this method, there is no need to know the spectral properties of target materials; also, no atmospheric or radiometric correction is required. PCA must be applied on raw and unstretched data for effective outcomes in all cases. Final images from PCA are accurate and sufficient in delineating alteration zones and also lithological differences.

Since principal component analysis (PCA) is an outcome of non-correlated components obtained through the analysis of all data set and axes of transferred new data with greatest amount of variation, the eigenvectors show the direction of each PC axis and the eigenvalues are for the variability of the data along the orthogonal directions (Chavez 1989; Gupta 2003). Thus, the magnitude and sign of eigenvector loadings (eigenvalues) give information about which spectral properties of vegetation, rocks, and soils are responsible for the statistical variance mapped into each PC, and this is the basis of the Crosta technique.

Here in the study, Crosta PCA using six bands was firstly applied to the Landsat scene of the study area. The composite image of PC4, PC3, and PC2 from PCA of Landsat's six reflected bands is the outcome image showing the basalts in the studied area (Kula) better than those appearing in the other composite images of PCs and in light brown color and, in some extent, separates the basalts from the neighboring areas (Fig. 4a), but not as clearly as expected. The results show that clearly, in any cases, it is not possible to separate mineral classes into any single principal component image when the method is applied to six TM bands (1, 2, 3, 4, 5, and 7). Consequently, the number of input channels is reduced to avoid a particular spectral contrast, and the chances of defining a unique principal component for a specific mineral class will be increased.

Selective PCA can be used to reduce the dimensionality of a data set. Thus, while minimizing the loss of information, the spectral contrast can be enhanced and mapped between two different spectral regions. The increase in the correlation between two TM bands is related to the amount of spectral contrast between them. Higher correlation between the spectral bands means less contrast and the lower correlation means more contrast (Chavez and Kwarteng 1989). Feature-oriented principal component selection depends on analyses of PCA eigenvector loadings which are directly related to the theoretical spectral signatures of specific targets. Thus, it can be decided which of the principal component will extract that information. The methodology mainly relies on selection of only four TM bands to perform PCA. This technique uses four selected TM bands in order to highlight the spectral response of, for example, iron oxide minerals (showing absorption in visible TM bands 1 and 2 and higher reflection in TM3) and hydroxyl-bearing (clay) minerals (showing absorption in TM7 and higher reflectance in TM5).

In the principal component transformation of Landsat TM images in the way of using two sets of four out of six reflected input bands, the result shows the first component as PC1 having a predictably high eigenvalue. Thus, it represents most of the variation within the whole dataset. This PC1 also provides information mainly on the albedo and the topography (Gupta 2003). The second, third, and fourth principal components represent progressively less variation within the datasets. For further knowledge of the analyses, readers are referred to Crosta and Moore (1989); so, the use of feature-oriented PCA technique in hydroxyl minerals and ferric minerals discrimination has been well established by Crosta and Moore (1989) and also by Loughlin (1991).

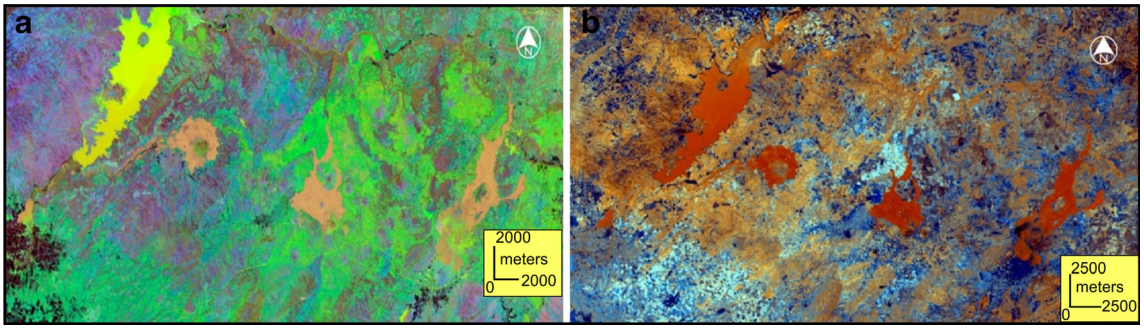

Fig. 4 **a** PCA result of Crosta technique using all Landsat bands (1 to 7 except 6). **b** PCA result of Crosta technique using two groups of Landsat bands (1, 3, 4, and 5, and 1, 4, 5, and 7)

In hydroxyl mapping, TM bands 1, 4, 5, and 7 are used. To avoid mapping the iron oxides, TM bands 2 and 3 are not considered, but instead of TM1, either of them could substitute. As it is mentioned previously, the analysis showed that the albedo (reflectance) is mapped by PC1, and the spectral difference between shortwave infrared and visible ranges is mapped by PC2. PC3 is found to be responsible for displaying the vegetation as the brightest object and PC4 highlights hydroxyl-bearing minerals as dark pixels. To map the hydroxyls in bright pixels, PC4 is negated (multiplied by −1) and called Crosta hydroxyl (H) image (Loughlin 1991).

One very important property of this H image is that it has a negative contribution from vegetation in TM4 (when negated), and therefore, vegetated areas are not highlighted and separated (Tangestani and Moore 2002).

Similarly, the iron oxide map is obtained by using the unstretched TM bands of 1, 3, 4, and 5. The substitution of TM5 with TM7 results with little effect. The principal components can be interpreted as albedo in PC1, difference between SWIR and visible spectral ranges in PC2, vegetation in PC3, and iron oxide minerals in PC4 as bright pixels after negation. So, PC4 of this transformation is called Crosta iron oxide image (F). Iron oxides could also be mapped in PC2 with hydroxyls; therefore, the eigenvector loadings of the iron oxide and hydroxyl sensitive bands (TM1, 3 and 5) should be checked considering the vegetation band of TM4 (Tangestani and Moore 2002).

The information in the H and F images can be combined to produce a map displaying the pixels with anomalous concentrations of both hydroxyls and iron oxides as the brightest. This new image is called H+F image. Therefore, a new PCA is applied to these two images to achieve, for example, the principal component having positive eigenvalues from these two input bands.

By using the Crosta H, H+F, and F images, which are stretched, color composites are prepared in desired combinations. Display of H, H+F, and F images in RGB channels respectively returns a dark bluish color composite image on which alteration or alumina-riched zones are unusually bright. White pixels within these zones are the areas both iron-stained and argillized. Bright reddish to orange zones are more argillized than iron-stained, and bright cyan to bluish zones are more iron-stained than argillized (Loughlin 1991) (Fig. 4b).

PCs from PCA providing essential statistical analysis of the spectral bands and with large amount of possible spectra information and even in color composites support the selection of correct ratio images in the lithological mapping. The magnitude and sign (positive or negative) of eigenvector loadings (e.g., eigenvalues) give information about which spectral properties of rocks are responsible for the statistical variance defined by each component (Rajesh 2008). In this case study, the fourth component (PC4) carries a high positive contribution (0.6454668) from TM1 and a high negative contribution (−0.5458363) from iron oxide highlighted in TM3, since iron oxide has a strong absorption in TM1 and high reflectance in TM3 (Table 1). On the other hand, ferric oxides were mapped to PC4 in the 1-3-4-5 band combination, and hydroxyls were mapped to PC4 in the other combination (using 1-4-5-7 band combination) with a high negative contribution (−0.5924913) from TM5 and a high positive contribution (0.7288171) from TM7 (Table 1). Crosta suggests taking these two PC4 into further PCA, and the product of PC2 from this final PCA is used to form the final RGB image together with those two previous PC4s (Fig. 4b). However, this is not a general rule for PC4.

Table 1 Eigenvalues of PCA of two Landsat band sets: 1, 3, 4, and 5, and 1, 4, 5, and 7 bands

Landsat bands	PC1	PC2	PC3	PC4
TM1	0.4293	−0.6022	−0.1908	0.6454668
TM3	0.5204	−0.0059	−0.6566	−0.5458363
TM4	0.3682	−0.4431	0.6768	−0.4582597
TM5	0.6397	0.6640	0.2726	0.2746514
TM1	0.4332	0.6068	−0.6454	−0.1658332
TM4	0.3748	0.5451	0.6870	0.3004646
TM5	0.6624	−0.4033	0.2176	−0.5924913
TM7	0.4826	−0.4145	−0.2531	0.7288171

In some other studies, it was mentioned that the inverse of PC4 enhanced hydroxyls if the combination of bands 1, 2, 3, 4, 5, and 7 was used as input to PCA, like proposed by Gupta (2003) and in a case study from central Mexico (Ruiz-Armenta and Prol-Ledesma 1998). On the other hand, it has been proposed as a general rule that the ratio image of TM5/TM4 detects the ferrous minerals as bright signs (Rawashdeh et al. 2006; Rajesh 2008). The PCA technique was used to discriminate the ferrous minerals, as for the ferric mineral enhancement. This confirms the results obtained by using ratio images. Mapping the Kula volcanic field uses the color composite of ratio images 3/1, 4/5, and 3/2 (RGB). It illustrates multifaceted information and provides higher contrast between the volcanic sheets (Fig. 3a).

Although the PC images in initially stretched forms provided brighter images and distinctive lithological units, they are found very similar to those of unstretched data, and a disturbance of other features prevented the enhancement of the alteration.

Results and discussions

As it became a well-known procedure using 7-5-3, 5-3-1, and 4-7-2 Landsat TM band images in lithological studies (Yazdi et al. 2011), all those RGB band combinations were examined, and 4-7-2 band combination was found to be the best among them for the Kula region. Color composite display of bands 4, 7, and 2 respectively in red, green, and blue channels is shown in Fig. 2a. The red areas are vegetated areas as the band 4 is sensitive to vegetation. Band 7 is responsible for moderate reflectance for clay minerals and is displayed in very light green and greenish colors. It is easy to say that band 7 could recognize the clay altered zones as there are various light green areas in the image. However, light green areas in the near vicinity of Kula volcanics are probably because of iron oxides or iron silicate more than clay alterations.

The bands 4 and 7 in red and green channels and band 5 in the blue channel produced a color composite image having clay-altered areas displayed as white. Iron-oxidized areas are displayed as green-cyan tones since iron oxides relatively have the same amount of reflectance in bands 5 and 7. Both vegetation and hydroxyls are reflective in band 4 interval. Thus, red areas are the vegetated and whitish pixels are clay dominant altered regions (Fig. 2b).

As the result shows, the color composite method is quick but not fully enough to delineate the certain borders for basalts. Only general information can be gathered. The procedure of assigning the bands to the display channels is the same in the other methods, changing the input bands to be displayed.

No image correction procedure has been applied to the images prior to the processes here in this study. Images selected for the display as a composite are histogram type contrast stretched. Histogram type contrast enhancement gives visually better display results than linear contrast stretching. That is because the stretching transformation is performed varyingly according to the histogram density in normalizing contrast enhancement.

Generally, the TM 5 and 7 bands (shortwave infrared I and shortwave infrared II) are highly correlated TM bands. However, the pair of TM 1 and 3 bands (blue and red) represents a lower correlation than other visible band pairs. Similarly, the pair of TM 4 and TM5 bands (near-infrared and shortwave infrared I) shows a lower correlation than most other pairs. These pairs are the best for rationing image investigation. As it is given in one of the previous sections, the rationing technique highlights the differences of the spectral absorption effects and also reduces errors caused by illumination and topography and thus facilitates the mapping of the lithology and the alteration zones.

The band ratio 3/1 effectively maps iron alteration minerals showing maximum reflectance within Landsat TM band 3 and minimum reflectance within Landsat TM band 1. Therefore, Landsat TM band ratio 3/1 increases the differences between the digital numbers (DNs) of iron alteration zones and those of unaltered rocks respectively (Sabins 1999). This leads to a better discrimination between basalts and other rock types in the present area. As Gupta (2003) also suggested in his study, to examine the existence of ferric minerals in this research on Kula volcanic basalt field, 3/1 ratio was computed, and results are shown in Fig. 5a. Two zones are identified within the region. According to ratio image, the volcanic rocks appear brighter than those of Kula landscape.

On the other hand, by investigating ferrous minerals using ratio 5/4 (Rawashdeh et al. 2006), the area can be separated into four regions from broken white to black (Fig. 5b). However, when ratio band image 5/7 is analyzed, the clay minerals appear in bright gray colors on the image (Sabins 1999), showing three main zones (ranging from a light gray color to dark gray) within the Kula basalt region (Fig. 5c). The band 5/7 ratio is sensitive to the hydroxyl mineral content of the rocks, such that areas of high 5/7 values have relatively high hydroxyl mineral contents (Kusky and Ramadan 2002). Band ratio of 5/7 is therefore expected to be emphasizing the clay minerals that give high reflectance in band 5 and relatively low in band 7. Ratio of band 3/2 gives high values for iron oxide minerals and band ratio of 4/5 gives very low values for iron oxides and nearly identical for clay minerals. Assigning respectively these ratios to the red, green, and blue channels, Fig. 4 is then obtained. Simply, the red pixel areas are clay-rich, green pixels are iron oxide, and blue pixels are both clay and iron oxide dominated areas. Yellow pixels represent hydrothermally altered clay and FeO-rich areas.

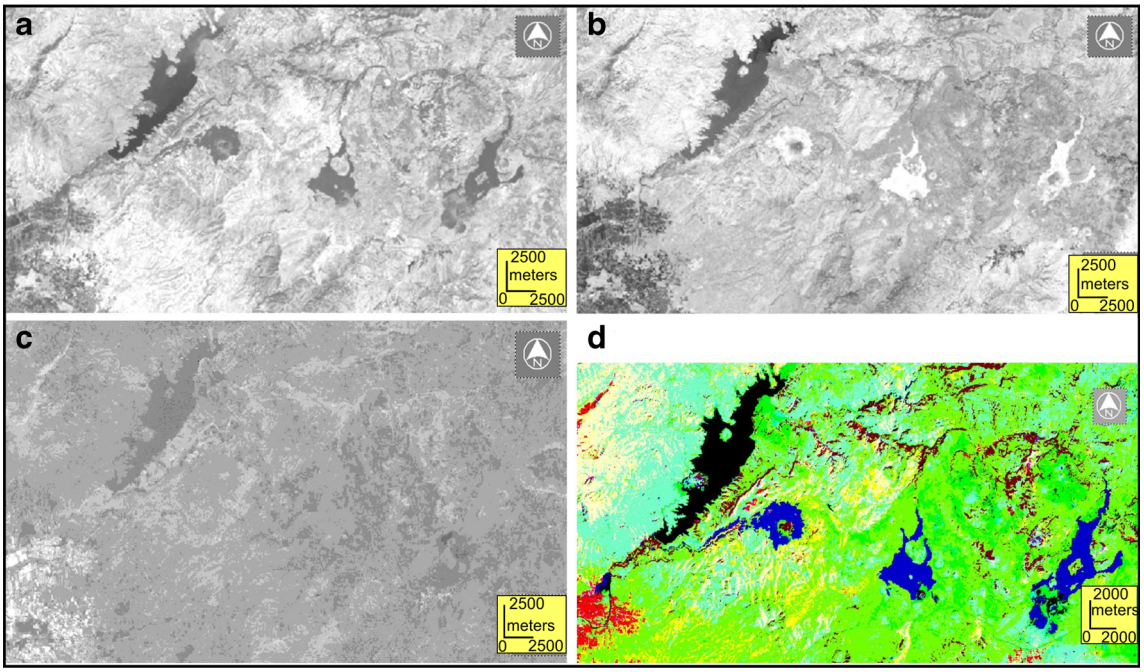

Fig. 5 **a** Gray tone image of 3/1 bands ratio. **b** Gray tone image of 5/4 bands ratio. **c** Gray tone image of 5/7 bands ratio. **d** RGB combination of PC3, PC2, and PC1 of the first, the third, and the first group ratio images, respectively

Basalt pattern mapping by PCA of Landsat band ratios

The boundaries between mantle and crustal lithologies are not very sharp due to different degrees of weathering and alteration. The developed band ratio is efficient in the discrimination of alteration zones and associated rock types in providing very subtle information based on the spectral sensitivity of different proportions of minerals contained in different rocks. However, the zones of mineralization were not clearly discriminated in the image, and thus, here an attempt is made to use principal component analysis (PCA) which has been widely used for mapping of zones of mineralization and alterations (Amer et al. 2010; Crosta et al. 2003; Crosta and Moore 1989; Gabr et al. 2010; Gad and Kusky 2006; Jing and Panahi 2006; Loughlin 1991; Madani et al. 2008; Rokos et al. 2000; Tangestani and Moore 2002).

Principal component analysis is also widely used for mapping of alteration in metallogenic provinces (Ranjbar et al. 2004). In the resultant image, all intensely hydrothermally altered areas are shown as bright pixels. This technique is used on four bands (bands 1, 3, 4, and 5 for enhancing iron oxides and bands 1, 4, 5, and 7 for enhancing hydroxyls). The only disadvantage in using this method on four bands is that the sedimentary rocks and the areas with mild hydrothermal signatures are also enhanced in the resultant image (Ranjbar et al. 2004).

On the other hand, here in this study, it was done several attempts if these "four-band" PCAs work for the basalts in Kula region well. As already shown and mentioned previously, they worked somehow. To improve these results and to get more reasonable and satisfying outcomes for delineating the boundaries of the basalts in the area, not only PCAs of these

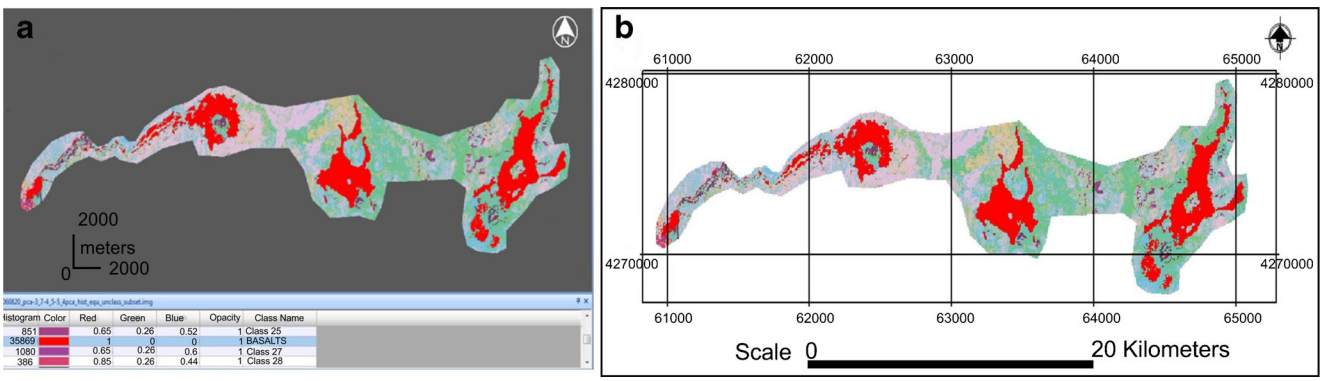

Fig. 6 **a** Subsetted image for basalt area after classification. **b** Map of the Kula basalts

two sets of four Landsat bands but also PCAs of some ratios that give results for discrimination of the basalts in the area better than other ratios were studied. Thus, here in this study, three separate principal component analyses were also performed for three groups of combined ratio images. The first group consists of 5/4, 5/1, and 3/7 ratio images, the second is for 7/4, 5/1, and 4/3, and final group is for the ratios of 3/1, 4/5, and 3/2. After these three PC analyses, some combination image of PCs from the first and the third groups except the second gave better RGB display result. Figure 5d shows that image consisting of the third PC (PC3) of the first group assigned to red and the second PC (PC2) of the third group to green and the first PC (PC1) of the first group to blue. The basalt areas appear as bright areas in the first PC (PC1) of the first group, and the same basaltic areas are therefore clearly highlighted as blue colors in the RGB image composed of these three PCs. Eigenvalue table of these three PCAs shows the maximum opposite loads from the second component (PC2) of the third PCA group and from the first component (PC1) of the second PCA group and from the third component (PC3) of the first PCA group (Table 1).

As it is well known, ground sampling distance (GDS) of a multispectral Landsat ETM+ image is 30 m by 30 m. Then, one Landsat image cell covers a 0.09-ha area on the ground. In the classified image in Fig. 6a, the total number of basalt pixels is obtained as 35,968 pixels. So basalts cover totally 3228 ha in the Kula region. Ortho-rectified image map of the Kula basalts can also be seen in Fig. 6b.

Conclusions

As a result, the color composite method is quick but not fully enough to delineate the certain borders for basalts. Only general information can be gathered. The procedure of assigning the bands to the display channels is the same in the other methods, changing the input bands to be displayed.

According to principal component analyses, these analyses were performed on three groups, each combining three ratio images. The first group consists of 5/4, 5/1, and 3/7 ratio images, the second is for 7/4, 5/1, and 4/3, and final group is for the ratios of 3/1, 4/5, and 3/2. After PC analyses of these three groups, some combination image of PCs from the first and the third groups except the second gave better RGB display result. RGB image composite of these three components with maximum opposite loads does not show a fine result for the basalt areas, but the combination image of the third PC (PC3) of the first group and the second PC (PC2) of the third group and then the first PC (PC1) of again the first group does. Thus, basalt areas are seen clearly in blue colors in Fig. 5d.

Future study is going to focus on determining the changes in the field coverage of the basalt region in Kula in time and those caused by human activities such as those done for rural, agricultural, or settlement purposes in the region. Satellite imagery and appropriate remote sensing analysis techniques are going to be chosen to determine the changes.

Acknowledgments The authors thank Professor Abdullah M. Al-Amri for his editorial handling of the manuscript and the anonymous referees for their detailed and constructive reviews. Satellite images of this study were processed in Image Processing Laboratory of the Geomatics Department of Gumushane University.

References

Abdelhamid G, Rabba I (1994) An investigation of mineralized zones revealed during geological mapping, Jabal Hamra Faddan-Wadi Araba, Jordan, using Landsat TM data. Int J Remote Sens 15(7): 1495–1506

Abdelsalam MG, Stern RJ, Berhane WG (2000) Mapping gossans in arid regions with Landsat TM and SIR-C images: the Beddaho Alteration Zone in northern Eritrea. J Afr Earth Sci 30(4):903–916

Abrams MJ, Brown D, Lepley L, Sadowski R (1983) Remote sensing for porphyry copper deposits in southern Arizona. Econ Geol 78:591–604

Amer R, Kusky TM, Ghulam A (2010) Lithological mapping in the Central Eastern Desert of Egypt using ASTER data. J Afr Earth Sci 56(2–3):75–82. doi:10.1016/j.jafrearsci.2009.06.004

Assiri A, Alsaleh A, Mousa H (2008) Exploration of Hydrothermal Alteration Zones Using ASTER Imagery: A case study on Nuqrah Area, Saudi Arabia. Asian J Earth Sci 2:1819–1886

Bishta AZ, Sonbul AR, Kashghari W (2014) Utilization of supervised classification in structural and lithological mapping of Wadi Al-Marwah Area, NWArabian Shield, Saudi Arabia. Arab J Geosci 7: 3855–3869. doi:10.1007/s12517-013-1044-9

Buckingham WF, Sommer SE (1983) Mineralogical characterization of rock surfaces formed by hydrothermal alteration and weathering-application to remote sensing. Econ Geol 78:664–674

Carranza EJM (2002) Geologically-Constrained Mineral Potential Mapping: Example from the Philippines. PhD Thesis, International Institute of Aerospace Survey and Earth Science (ITC)

Carranza EJM, Hale M (1999) Image processing and GIS for hydrothermal alteration mapping, Baguio district, Philippines. Proceedings of the 1999 I.E. International Geoscience and Remote Sensing Symposium, Hamburg, Germany, 28 June-2 July (on CDROM)

Chavez PS (1989) Radiometric calibration of Landsat Thematic Mapper multispectral images. Photogramm Eng Rem S 55(9):1285–1294

Chavez PS, Kwarteng AY (1989) Extracting spectral contrast in Landsat Thematic Mapper image data using selective principal components analysis. Photogramm Eng Rem S 3:339–348

Chica-Olmo M, Abarca F (2002) Development of a Decision Support System based on remote sensing and GIS techniques for gold-rich area identification in SE Spain. Int J Remote Sens 23(22):4801–4814

Crosta AP, Moore JM (1989) Enhancement of Landsat Thematic Mapper imagery for residual soil mapping in SW Minas Gerias state, Brazil: a prospecting case history in Greenstone belt terrain. Proceeding of the Ninth Thematic conference on Remote Sensing for Exploration Geology, Calgary, Alberta, Canada, 2-6 October, pp. 1173-1187

Crosta AP, De Souza Filho CR, Azevedo F, Brodie C (2003) Targeting key alteration minerals in epithermal deposits in Patagonia, Argentina, using ASTER imagery and principal component analysis. Int J Remote Sens 24:4233–4240

Darning WP (1998) Affiliated Research Center, Integrated Use of Remote Sensing and GIS for Mineral Exploration. Final Report, pp 3 – 4

Drury SA (1993) Image interpretation in Geology. Chapman and Hall, London

Drury SA, Hunt GA (1989) Geological uses of remotely-sensed reflected and emitted data of lateralized Archaean terrain in Western Australia. Int J Remote Sens 10:475–497

El Janati M, Soulaimani A, Admou H, Youbi N, Hafid A, Hefferan KP (2014) Application of ASTER remote sensing data to geological mapping of basement domains in arid regions: a case study from the Central Anti-Atlas, Iguerda inlier, Morocco. Arab J Geosci 7: 2407–2422. doi:10.1007/s12517-013-0945-y

Ercan T (1984) Geology of Kula area and petrology of Kula volcanics. Ph.D Thesis, Istanbul University

Ferrier G, Griffiths KWG, Bryant R, Stefouli M (2002) The mapping of hydrothermal alteration zones on the island of Lesvos, Greece using an integrated remote sensing dataset. Int J Remote Sens 23:1–16

Gabr S, Ghulam A, Kusky T (2010) Detecting areas of high-potential gold mineralization using ASTER data. Ore Depos Rev 38:59–69

Gad S, Kusky T (2006) Lithological mapping in the Eastern Desert of Egypt, the Barramiya area, using Landsat thematic mapper (TM). J Afr Earth Sci 44:196–202

Gupta RP (2003) Remote Sensing Geology. Springer-Verlag, Berlin

Hassan SM, Ramadan TM (2014) Mapping of the late Neoproterozoic Basement rocks and detection of the gold-bearing alteration zones at Abu Marawat-Semna area, Eastern Desert, Egypt using remote sensing data. Arab J Geosci. doi:10.1007/s12517-014-1562-0

Holness MB (2005) Spatial constraints on magma chamber replenishment events from textural observations of cumulates: the Rum Layered Intrusion Scotland. J Petrol 46:1585–1601

Holness MB, Bunbury JM (2006) Insights into continental rift related magma chambers: igneous nodules from the KulaVolcanic Province, Western Turkey. J Volcanol Geoth Res 153:241–261

Hunt GR (1979) Near-infrared (1.3–2.4 μm) spectra of alteration minerals: potential for use in remote sensing. Geophysics 44:1974–1986

Jensen JR (1996) Introductory Digital Image Processing: A Remote Sensing Perspective. Prentice-Hall, New Jersey

Jing QCL, Panahi A (2006) Principal component analysis with optimum order sample correlation coefficient for image enhancement. Int J Remote Sens 27:3387–3401

Kaufmann H (1988) Mineral exploration along the Agaba-Levant structure by use of TM-data concepts, processing and results. Int J Remote Sens 9:1630–1658

Kusky TM, Ramadan TM (2002) Structural controls on Neoproterozoic mineralization in the South Eastern Desert, Egypt: an integrated field, Landsat TM, and SIR-C/X SAR approach. J Afr Earth Sci 35:107–121

Liu F, Wu X, Sun H, Guo Y (2007) Alteration information extraction by applying synthesis processing techniques to Landsat ETM $^{+}$ data: case study of Zhaoyuan Gold Mines, Shandong Province, China. J China Univ Geosci 18:72–76

Loughlin WP (1991) Principle components analysis for alteration mapping. Photogramm Eng Rem S 57:1163–1169

Madani A, Bishta A (2002) Selection of the optimum bands of Landsat-7 ETM+for automatic lineaments extraction: a case study of Qattar Granites, North Eastern Desert, Egypt. 6th International Conference on the Geology of the Arab World, 6. Cairo University, pp. 353–360

Madani A, Abdel Rahman EM, Fawzy KM, Emam A (2003) Mapping of the hydrothermal alteration zones at Haimur Gold Mine Area, South Eastern Desert, Egypt using remote sensing techniques. Egypt J Remote Sens Space Sci 6:47–60

Madani A, Harbi H, Eldougdoug A (2008) Utilization of remote sensing techniques for mapping the listwaenite associated with Jabal Al-Wask Ophiolite Complex, Northwestern Saudi Arabia. Egypt J Remote Sens Space Sci 11:57–72

Moore CA, Hoffmann GA, Glenn NA (2007) Quantifying basaltic rock outcrops in NRCS Soil Map Units Using Landsat-5 Data. Soil Surv Horiz 48:59–63

Pournamdari M, Hashim M (2014) Detection of chromite bearing mineralized zones in Abdasht ophiolite complex using ASTER and ETM^{+} remote sensing data. Arab J Geosci 7:1973–1983. doi:10.1007/s12517-013-0927-0

Qari MHT (2011) Utilizing image processing techniques in lithologic discrimination of Buwatah area, Western Arabian Shield. Arab J Geosci 4:13–24. doi:10.1007/s12517-009-0049-x

Raines GL, Offield TW, Santos ES (1978) Remote sensing and subsurface definition of facies and structure related to uranium deposits Powder River Basin. Wyoming Econ Geol 75:1706–1725

Rajesh HM (2008) Mapping Proterozoic unconformity related uranium deposits in the Rockhole area, Northern Territory, Australia using landsat ETM^{+}. Ore Geol Rev 33:382–396

Ramadan TM, Kontny A (2004) Mineralogical and structural characterization of alteration zones detected by orbital remote sensing at Shalatein District, SE Desert, Egypt. J Afr Earth Sci 40:89–99

Ramadan TM, Abdelsalam MG, Stern RJ (2001) Mapping gold-bearing massive sulfide deposits in the Neoproterozoic Allaqi Suture, Southeast Egypt with Landsat TM and SIR-C/X SAR images. Photogramm Eng Rem S 67(4):491–497

Ranjbar H, Honarmand M, Moezifar Z (2004) Application of the Crosta technique for porphyry copper alteration mapping, using ETM data in the southern part of the Iranian volcanic sedimentary belt. J Asian Earth Sci 24:237–243

Rawashdeh SA, Saleh B, Hamzah M (2006) The use of remote sensing technology in geological investigation and mineral detection in El Azraq-Jordan. Cyber Geo 12(11):1–22

Richardson-Bunbury JM (1996) The Kula Volcanic Field, Western Turkey: the development of a Holocene alkali basalt province and the adjacent normal faulting graben. Geol Mag 133:275–283

Rokos D, Argialas D, Mavrantza R, St.-Seymour K, Vamvoukakis C, Kouli M, Lamera S, Paraskevas H, Karfakis I, Denes G (2000) Structural mapping and analysis for a preliminary investigation of possible gold mineralization by using remote sensing and geochemical techniques in a GIS environment: study area: island of Lesvos, Aegean Sea, Hellas. Nat Resour Res 9:277–293

Rothery DA (1987) Improved discrimination of rock units using Landsat Thematic Mapper imagery of the Oman ophiolite. J Geol Soc London 144:587–597

Rowan LC, Bowers TL (1995) Analysis of linear features mapped in Landsat thematic mapper and side-looking airborne radar images of the Reno, Nevada 18 by 28 quadrangle, Nevada and California - implications for mineral resource studies. Photogramm Eng Rem S 61:749–759

Rowan LC, Wetlaufer PH, Goetz AFH, Billingsley FC, Stewart JH (1977) Discrimination of rock types and detection of hydrothermally altered areas in south-central Nevada by use of computer-enhanced ERT images. US Geological Survey Professional Paper 883

Ruiz-Armenta JR, Prol-Ledesma RM (1998) Techniques for enhancing the spectral response of hydrothermal alteration minerals in Thematic Mapper images of Central Mexico. Int J Remote Sens 19(10):1981–2000

Sabins FF (1999) Remote sensing for mineral exploration. Ore Geol Rev 14(3-4):157–183

Salem SM, Soliman NM, Ramadan TM, Greiling RO (2014) Exploration of new gold occurrences in the alteration zones at the Barramiya District, Central Eastern Desert of Egypt using ASTER data and geological studies. Arab J Geosci 7:1717–1731. doi:10.1007/s12517-013-0874-9

Sultan M, Arvidson RE (1986) Mapping of serpentinites in the Eastern Desert of Egypt by using Landsat Thematic Mapper data. J Geol 14(12):995–999

Tangestani MH, Moore F (2002) Porphyry copper alteration mapping at the Meiduk area, Iran. Int J Remote Sens 23(22):4815–4825

Tokcaer M, Agostini S, Savascin MY (2005) Geotectonic Setting and Origin of the Youngest Kula Volcanics (Western Anatolia), with a New Emplacement Model. Turkish J Earth Sci 14:145–166

Vincent RK (1997) Fundamentals of Geological and Environmental Remote Sensing. Prentice Hall, New Jersey

Warner NH, Farmer JD (2008) Laboratory and Remote Identification of Hydrothermal Alteration Materials Associated with Subglacial Outflood Surfaces in Iceland. Lunar and Planetary Science, p. 1477

Yazdi M, Sadati N, Matkan AA, Ashoorloo D (2011) Application of Remote Sensing in Monitoring of Faults. Int J Environ Res 5(2): 457–468

Youssef AM, Hassan AM, El Moneim Mohamed MA (2009) Integration of remote sensing data with the field and laboratory investigation for lithological mapping of granitic phases: Kadabora pluton, Eastern Desert, Egypt. Arab J Geosci 2:69–82. doi:10.1007/s12517-008-0020-2